Materials Research Bulletin 44 (2009) 130–133

Contents lists available at ScienceDirect

Materials Research Bulletin

journal homepage: www.elsevier.com/locate/matresbu

Floating combustion synthesis of spherical vitreous silica nano-powder

Yuan Zhu [a], Hai Bo Jin [b], Ke Gang Ren [a], Simeon Agathopoulos [c], Ke Xin Chen [a,*]

[a] State Key Laboratory of New Ceramics and Fine Processing, Department of Materials Science and Engineering, Tsinghua University, Beijing 100084, PR China
[b] School of Materials Science and Engineering, Beijing Institute of Technology, Beijing 100081, PR China
[c] Department of Materials Science and Engineering, University of Ioannina, Greece

ARTICLE INFO

Article history:
Received 5 December 2007
Received in revised form 22 February 2008
Accepted 15 March 2008
Available online 8 April 2008

Keywords:
A. Amorphous materials
A. Oxides
C. Electron microscopy

ABSTRACT

Vitreous silica nano-powder, with spherical particles of 50–300 nm in size, was successfully produced via floating combustion synthesis. Mechano-chemically activated and spray-dried Si-powder was oxidized in fluidized bed between 900 °C and 1550 °C in air. After 10 min, rapid removal of powder from the furnace and quenching maintained silica's vitreous nature. The process comprises sequential cycles of the following stages until nano-sized particles of silica are obtained. Superficial melting of Si-particles initially occurs and the particles obtain a spherical shape. The surface of the particles is oxidized. The stress at silica/silicon interface causes collapse of particles to smaller ones.

1. Introduction

Floating combustion synthesis is a modern low-cost method for industrial production of high quality ceramic powders because of the simple equipment and installation, low energy consumption, and short processing time. It actually combines combustion synthesis and fluidized bed [1,2].

In the production of silicon nitride with floating combustion synthesis in fluidized bed, where silicon particles react with nitrogen, the process is largely based on the progressive collapse of bigger particles to smaller ones during the process due to the stresses developed at the interface between the surface-crystalline-Si_3N_4 and the bulk-Si of particles' core [3]. Microwave-assisted combustion synthesis of Ta_2N in fluidized bed has been also carried out [4]. Our research team has applied this technique to produce high quality Si_3N_4 and TiC_xN_y hyper-fine powders [5].

Nowadays, nano-powders are highly demanded for producing high quality materials for many advanced applications. In the particular case of silica, nano-powders of spherical vitreous silica have high potential in electric and electronic applications because of the high dielectric constant and thermal moisture resistance, as well as the low thermal expansion, residual stresses, and friction [6]. Other applications, such as biomedical, electrical, magnetic, and structural ones, should be also added in the list. Accordingly, this paper presents experimental results of successful production of spherical vitreous silica nano-powder with floating combustion synthesis in an industrial-scale plant. The results are discussed in order to shed light in the stages of the process.

2. Materials and experimental procedure

The silicon powder (>45 μm, Dadizelin Co. Ltd., Beijing) was first subjected to pretreatment of mechano-chemical activation [7] and then spray-dry [8]. In particular, silicon powder was mixed with 1 wt% NH_4Cl (dispersant) and then activated by dry grinding in a vibration-mill for 1.5 h. The activated silicon powder was spray-dried with 1 wt% poly-ethylen-oxide (binder).

The experimental setup is sketched in Fig. 1. The pretreated silicon powder enters the furnace with a flow rate of 20 l/min at atmospheric pressure. The temperature profile inside the furnace is 900 °C at the entrance and gradually rises up to 1550 °C (maximum) in the centre of the furnace. After 10 min, the powder is taken out from the furnace drifted from a strong air-flow in the cyclone, and then rapidly cooled (quenching) in the cooler.

The following methods and equipments were employed to characterize the materials. X-ray diffraction (XRD, Automated D/Max B, Rigaku) was used to determine the crystalline regime of the powder. Chemical analysis was carried out with the aid of X-ray fluorescence (XRF-1800, SHIMADZU). Observations of the microstructure were made with scanning electron microscopy (SEM, GSM-6460, JEOL, and FESEM, S-4300, Hitachi E1030) and transmission electron microscopy (TEM, 200CX, JEOL), equipped with energy dispersive X-ray spectroscopy (EDS) and selected area electron diffraction (SAED).

* Corresponding author. Tel.: +86 10 6277 2548; fax: +86 10 6277 2548.
E-mail address: kxchen@mail.tsinghua.edu.cn (K.X. Chen).

0025-5408/$ – see front matter © 2008 Elsevier Ltd. All rights reserved.
doi:10.1016/j.materresbull.2008.03.025

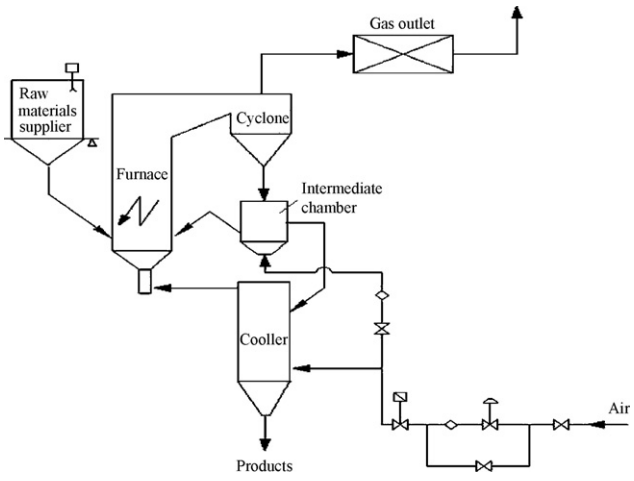

Fig. 1. Outline of the floating combustion synthesis plant.

3. Results

Fig. 2 shows the influence of pretreatment on morphology and particle size of Si-powder. Mechano-chemical activation was actually applied to lower the reaction temperature of the process. Nevertheless, the small average size of ~5 μm after mechano-chemical activation (Fig. 2a) is expected to favor development of cohesive forces among the particles. The big spherical Si-particles (~60 μm in diameter, Fig. 2b), obtained after spray-dry, anticipate good fluidity of powder at the entrance of furnace [9].

After the course of the process of Fig. 1, the resultant powder had white color. Its features are summarized in Fig. 3. The powder consisted of well-shaped spherical particles with a diameter of c.a. 50–300 nm (Fig. 3a). X-ray fluorescence analysis showed that the produced powder was slightly depleted of oxygen, i.e. mol ratio of Si/O = 1/1.95. The diffractogram of Fig. 3b confirms the presence of

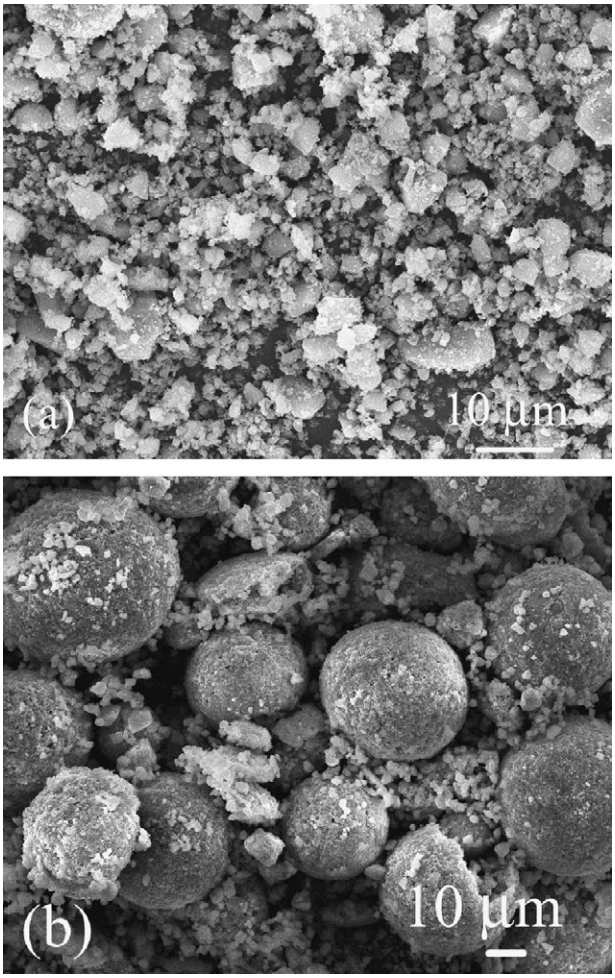

Fig. 2. Morphology of Si-powders after (a) mechano-chemical activation and (b) spray-dry.

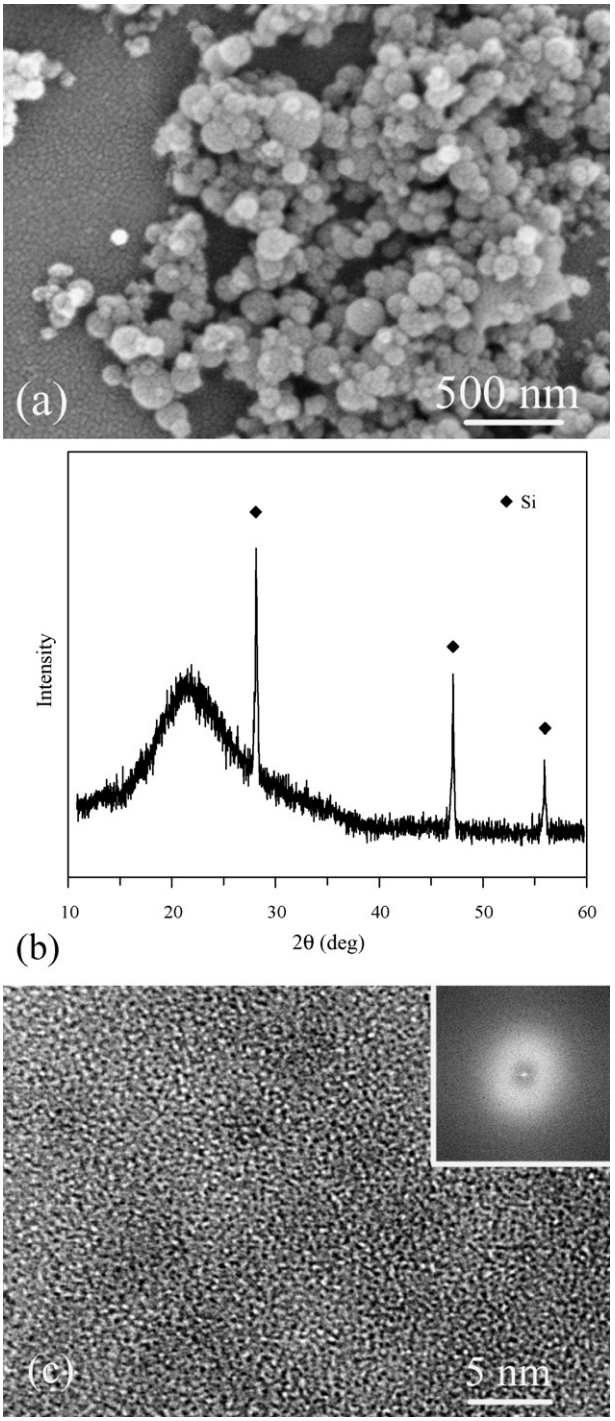

Fig. 3. (a) Morphology (FESEM) of the produced vitreous silica nano-particles, (b) their diffractogram, and (c) HRTEM image with SAED pattern (inset).

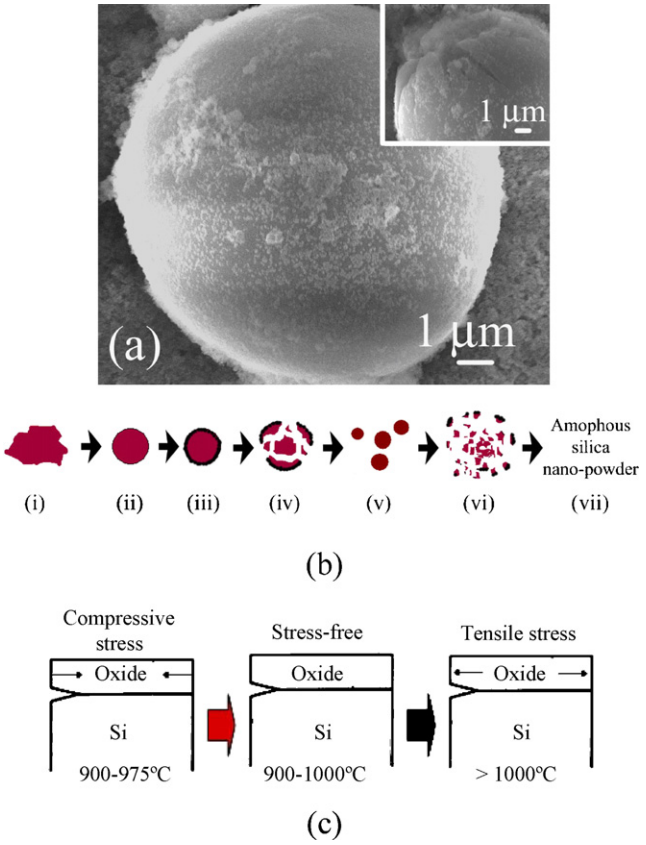

Fig. 4. (a) SEM image of a superficially melted Si-sphere and a similar sphere locally cracked at the surface (inset). (b) Schematic representation of the stages of the process. (c) Regimes of stresses at the Si/SiO_2 interface for different temperature ranges (note that a thin film of crystalline SiO_2 is also anticipated to form at the interface).

non-reacted Si in the produced powder, suggesting imperfect oxidation. However, it is worthy to note that the investigated processing completely suppresses formation of crystallized silica. The HRTEM image of Fig. 3c confirms the amorphous nature of the produced silica since the observed spots, presumably attributed to atomic level units, are randomly arranged. Moreover, the SAED pattern (inset of Fig. 3c) indicates an amorphous nature (since the patterns of crystallized nano-particles are broad but distinct rings).

To shed light in the stages of the process, we collected intermediate products after short reaction (oxidation) time, i.e. ~30 s. Fig. 4a shows a typical superficially oxidized Si microsphere with size of about 10 μm. We also observed many spheres whose surface was extensively but locally cracked (inset of Fig. 4a).

4. Discussion

According to the experimental results, the stages of the process can be depicted in Fig. 4b. When the silicon particles (Fig. 2b) enter the furnace, the organic binder immediately burns out (i.e. at 900 °C) and hence, the morphology of Si-particles must be close to Fig. 2a (stage i of Fig. 4b). Bulk Si melts at 1412 °C. However, earlier independent experiments (unpublished data, whose detail description is beyond the scope of the present paper) have shown that mechano-chemical activation causes reduction of superficial melting temperature of Si-particles at 900 °C. Therefore, the temperature at the entrance of the furnace was set at 900 °C. The melting at particles' surface layer expands because the particles travel towards the centre of the furnace (maximum temperature 1550 °C), that is further intensified because of the strong exothermic effect of the oxidation–combustion reaction of Si. The superficially molten particles spontaneously obtain spherical shape (stage ii) due to the effect of surface tension under a microgravity field (the fluidized bed conditions [10] balance the effect of gravity). Bigger particles (stage ii) are expected to be less spherical than smaller ones (stage v) because the shorter the radius the stronger the cohesive force ($\Delta p = 2\gamma/r$) [11]. Oxidation easily takes place at the molten surface layer of Si-particles (stage iii). The inevitably developed stresses at the SiO_2/Si interface, due to the lattice misfit and the mismatch of thermal expansion coefficients of the contacting phases, result in crack formation and propagation in the surface but also in the bulk of the particles (Fig. 4a). Therefore, the particles collapse in such a way as shown in the stage (iv) of Fig. 4b.

Accordingly, the collapse of the particles is a stage of high importance. The interface between the oxide layer and the core of silicon at three different temperature ranges is sketched in Fig. 4c. Qualitative earlier studies have suggested that a thin film of crystalline SiO_2 forms at the interface between Si and vitreous SiO_2 [12–14]. There is pronounced difference among the coefficients of thermal expansion (CTE) of crystalline SiO_2 ($15.6 \times 10^{-6}\,K^{-1}$) [15], vitreous SiO_2 ($0.58 \times 10^{-6}\,K^{-1}$) [16], and Si ($3.5 \times 10^{-6}\,K^{-1}$) [17]. However, it has been postulated [18] that this particular interface is stress-free between 975 °C and 1000 °C. This means that the stress due to CTE mismatch balances the stress due to lattice misfit within that narrow temperature range (i.e. 975–1000 °C). In other words, that stress-free regime suggests a transition stage, with regard to the type of the stresses dominating at the interface (i.e. due to lattice misfit or CTE mismatch). In the light of the big difference among the CTEs of the three phases (mentioned above), it would be assumed that the stress at the interface at temperatures higher than 1000 °C is due to CTE mismatch. The lower value of the CTE of vitreous silica (than the other two phases mentioned above) implies development of tensile stress at temperatures higher than 1000 °C. The maximum misfit strain, ε, between 1000 °C (i.e. the upper limit of the stress-free regime) and 1500 °C (i.e. the maximum temperature of the furnace) is calculated as

$$\varepsilon = (15.6 \times 10^{-6}\,K^{-1} - 0.58 \times 10^{-6}\,K^{-1})500\,K = 0.751\%$$

Assuming the stress-free regime (975–1000 °C) at the interface of Fig. 4c as a transition stage and the development of tensile stress at temperatures higher than 1000 °C, compressive stresses must be developed at temperatures lower than 975 °C, predominantly resulted from lattice misfit at the interface. Experimental results of thermal oxidation of silicon substrates, used in MEMS and VLSI processes, where stoichiometric dry oxidation took place at temperatures above 900 °C [19], support fairly well our hypothesis (the silica developed was also non-crystalline, similar to the silica produced in the present study). Compressive stresses of ~300 MPa were measured at room temperature [19].

The stages (ii)–(iv) of Fig. 4b are repeated (i.e. stages v and vi) until particle size is reduced down to nano-level. In our plant and with the given (in this study) materials' initial stage and pretreatment as well as processing conditions, this process lasts 10 min. Then, rapid cooling (which is feasible because of the whole experimental set up, based on fluidized bed concept) maintains the vitreous nature of the resultant silica powder (stage vii).

5. Conclusions

Floating combustion synthesis was successfully employed to produce vitreous silica powder with spherical nano-particles. The

process effectively suppresses the formation of crystalline silica, but traces of non-reacted silicon were detected by X-ray diffraction analysis. The pretreatments of mechano-chemical activation (to reduce the melting temperature of Si-particles) and spray-dry (to facilitate fluidity at the supply) are of crucial importance. The process in the furnace comprises sequential circles of the stages of surface melting of silicon particles at the micro-gravity conditions of fluidized bed, resulting in spherical particles, the oxidation of the surface, and the collapse of the particles due to developed stresses at the Si/SiO_2 interface. When the particles reach nano-size, the process ends with quenching, which maintains the vitreous nature of silica nano-powder.

Acknowledgements

The participation of S. Agathopoulos in this research and paper was done in the framework of the Project ENTER 04EP26, co-financed by E.U. (European Social Fund, 75%) and the Greek Ministry of Development (GSRT, 25%).

References

[1] Y.D. Liu, Fluidized-bed nitridation of silicon—direct use of very fine powder for alpha-silicon nitride production, Ph.D. Dissertation, Oregon State University, 1996.
[2] V. Pavarajarn, Roles of gas and solid components in the derect nitridation of silicon, Ph.D. Dissertation, Oregon State University, 2002.
[3] J. Koike, S. Kimura, J. Am. Ceram. Soc. 79 (2) (1996) 365–370.
[4] J. Akihl, K. Brezinsky, J. Am. Ceram. Soc. 86 (2) (2003) 222–226.
[5] J.T. Li, K.X. Chen, H.B. Jin, Floating combustion synthesis of Si_3N_4 and TiC_xN_y super-fine ceramic powders, Annual Report of the National High Technology Research and Development Program of China (863 Program), 2002.
[6] K.G. Ren, Study on combustion synthesis of high performance Si_3N_4 powders in large scale at low cost, Master Dissertation, Tsinghua University, 2005.
[7] A.N. Streletskii, I.V. Kolbanev, A.B. Borunova, Yu.P. Butyagin, Colloid J. 67 (5) (2005) 631–637.
[8] S.J. Luksiewicz, J. Am. Ceram. Soc. 72 (4) (1989) 617–624.
[9] D. Geldart, Gas Fluidization Technology, Wiley-Interscience Publication, U.K., 1986, pp. 33–37.
[10] D.R. Poirier, G.H. Geiger, Transport Phenomena of Materials Processing, TMS Press, PA, USA, 1994, p. 97.
[11] I.N. Levine, Physical Chemistry, 5th ed., McGraw-Hill Press, New York, USA, 2003 pp. 387–389.
[12] W.A. Tiller, J. Electrochem. Soc. 127 (1980) 619.
[13] W.A. Tiller, J. Electrochem. Soc. 127 (1980) 625.
[14] W.A. Tiller, J. Electrochem. Soc. 128 (1981) 689.
[15] G.Q. Liu, Handbook of Physical Properties in Chemistry & Chemical Engineering, Chemical Industry Press, Beijing, China, 2002, p. 275.
[16] J.A. Dean, Lange's Handbook of Chemistry, 13th ed., McGraw-Hill Press, New York, USA, 1985, p. 10.123.
[17] G.Q. Liu, Handbook of Physical Properties in Chemistry & Chemical Engineering, Chemical Industry Press, Beijing, China, 2002, p. 265.
[18] L.E. Katz, in: S.M. Sze (Ed.), VLSI Technology, 2nd ed., McGraw-Hill Press, New York, USA, 1984, pp. 131–157.
[19] M. Madou, Fundamentals of Microfabrication, CRC Press, New York, USA, 1997, pp. 92–96.